Observations of electron phase-space holes driven during magnetic reconnection in a laboratory plasma

W. Fox[*], M. Porkolab, J. Egedal, N. Katz, and A. Le

Department of Physics, and Plasma Science and Fusion Center,
Massachusetts Institute of Technology, Cambridge, MA 02139
(Dated: February 10, 2012)

This work presents detailed experimental observations of electron phase-space holes driven during magnetic reconnection events on the Versatile Toroidal Facility. The holes are observed to travel on the order of or faster than the electron thermal speed, and are of large size scale, with diameter of order 60 Debye lengths. In addition, they have 3-D spheroidal structure with approximately unity aspect ratio. We estimate the direct anomalous resistivity due to ion interaction with the holes and find it to be too small to affect the reconnection rate; however the holes may play a role in reining in a tail of accelerated electrons, and they indicate the presence of other processes in the reconnection layer, such as electron energization and electron beam formation.

I. INTRODUCTION

Electron phase-space holes [1, 2], are the self-consistent nonlinear plasma structures that form when a finite number of particles become trapped in large-amplitude plasma waves. They are well known, from simulations, to form out of two-stream or strong-beam-driven instabilities when the instability saturates by trapping electrons. They typically are found to form from strong current- or beam-driven turbulence.

Because of their connection with strongly-driven electron beams and strong plasma turbulence, it is not surprising that electron holes have been found in concert with sites of magnetic reconnection. Magnetic reconnection [3, 4] changes the topology of the magnetic field and thereby enables the explosive release of magnetic energy in solar flares, magnetospheric storms, and laboratory plasmas. The converted energy heats the plasma, drives high-speed jets, and accelerates particles. Magnetic reconnection is typically observed to occur much faster than can be explained by elementary resistive MHD theory, and therefore additional physics, such as two-fluid theory or anomalous, localized dissipation is required to boost reconnection rates to values observed. The fast rates of reconnection observed in these systems further imply the existence of very strong parallel electric fields, which can energize electrons [5].

Electron holes may play a role in these dissipation processes by scattering electrons and ions and thereby providing a source of anomalous drag. However, beyond their possible direct role in reconnection, their observation has other implications, namely they point to the existence of other physical processes in the reconnection region. For example, typically electron holes are found to arise from strong beam-on-tail instability, thus their ex-

istence points to strong electron beam formation by the reconnection event.

Electron holes were recently observed [6] by the authors in the Versatile Toroidal Facility (VTF) reconnection experiment at MIT [7]. Previous to these laboratory observations, electron holes had been launched and studied in detail in Q-machine plasmas [8–10] or in non-neutral plasmas [11], but no lab experiment had observed the self-consistent creation of electron holes from current-driven turbulence. Electron holes have now also been observed and studied in detail in an experiment where turbulence was driven by an externally launched electron beam [12].

Electron holes have been observed in a number of locations in the space environment, [13–15]. including in conjunction with reconnection both at the Earth's magnetopause [16] and in the magnetotail [17]. Most recently, electron holes with properties very similar to those observed in VTF have been observed in a bursty bulk-flow event (downstream of a reconnection site in the magnetotail) by the THEMIS spacecraft constellation [18]. These holes traveled with superthermal velocities and had large diameters (many 10's of λ_D).

Holes have also been found and studied in simulations of magnetic reconnection. Drake *et al.* [19] have found electron holes resulting from electron-ion (Buneman) instability in reconnection simulations, and argued that they were an important source of anomalous resistivity which aided the reconnection process. In more recent simulations, Che *et al* [20] found additional, superthermal electron holes which appeared at later times, which were shown to arise from electron-electron beam instability and which may have been instrumental in reining in a tail of fast electrons.

This paper presents additional, detailed measurements of the properties of the holes beyond those presented in Ref. [6]. Measurements of typical hole size, shape, and speed, have been repeated with substantially faster digitizing hardware. The higher resolution measurements confirm the basic width and speed measurements made

---

[*]Present address: Space Science Center, University of New Hampshire, Durham, NH 03824

with previous hardware, and allow more detailed investigation such as construction of the typical hole shape through conditional averaging. In addition, measurements have been taken with an electron energy-analyzing probe in close proximity to hole measurements, which show an increased population of high-energy electrons in concert with the holes.

We also present a detailed discussion of the observations. We present scaling arguments which demonstrate that the holes are electrostatic and connect our observations to other space observations and available theory, including a review of other possible non-linear theories to explain the positive spikes. We also present a simple quantitative estimate of the direct anomalous drag due to the holes, which indicates that their effects are small because the holes move too fast to efficiently couple electron and ion momentum. However, their role in reining in the tail of a runaway electron population or fast electron beams may well be important.

The remainder of this paper is organized as follows. Section II reviews the experimental setup of the VTF experiment. Section III presents typical observations of electron holes in VTF and their association with reconnection events. Section IV presents detailed measurements of individual holes, such as their size, shape, and speed conducted with both generations of digitizing hardware. Section V presents relevant discussions, including a scaling argument that the observed holes are predominantly electrostatic, an examination and rejection of other possible non-linear plasma structures to explain the observed phenomena, and connections to other recent observations and theory. Finally, Section VI presents the conclusions.

II. EXPERIMENTAL SETUP

The experimental setup is very similar to previous reconnection experiments on VTF [6, 7, 21, 22], and is depicted in Fig. 1.

Reconnection is studied in a regime of strong "guide" magnetic field, which is applied by toroidal field coils. For the experiments reported here, the toroidal guide field is 70 mT at the reconnection current sheet. An additional set of toroidal conductors fixed within the vacuum vessel generates the poloidal magnetic field, which in vacuum has a figure-8 geometry (Fig. 1). Experiments here used Ar plasma at fill pressures near 10^{-4} Torr. The plasma density reached $\sim 1 \ 10^{18}$ m^{-3}, with base electron temperatures (before reconnection) near 15 eV. (Throughout this paper many plasma parameters will be estimated based on this typical temperature, but it should be kept in mind that the temperature is observed to increase by about a factor of ~ 2 during the reconnection events, and possibly even more in localized regions near the electron hole turbulence under study.) Plasma is initiated with a microwave breakdown, after which the density and plasma current is built up by ohmic heating for about
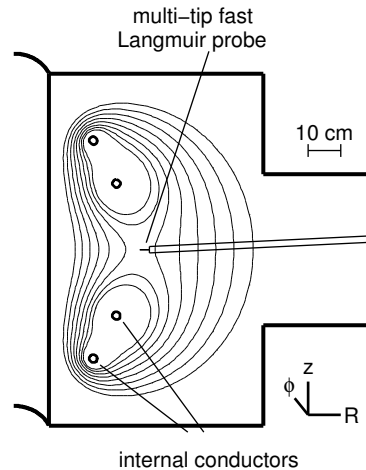

FIG. 1: A diagram at one poloidal cross section of VTF, showing internal field coils with vacuum flux surfaces and a fast (RF) Langmuir probes.

1 ms. Subsequently, a current sheet is driven by quickly changing the current in the toroidal conductors [7]. Typically the current sheet is metastable for ~ 100's of μs before undergoing a fast reconnection event in which the plasma current in the current sheet drops by nearly a factor of 2 over a time scale of about 10 μs.

Plasma fluctuations are observed with high-bandwidth, "fast" Langmuir probes [23]. The Langmuir probes are constructed using impedance-matched, semi-rigid cable (Micro-coax, Inc.), which carries the signals to a high-bandwidth digitizing oscilloscope. Up to four probe tips are deployed in a small area. When arrayed along the magnetic field, which is also the direction of the dominant electron current flow, cross correlation techniques can be used to observe the parallel phase velocity of the observed fluctuations, or in the case here, the parallel velocity of the electron hole structures.

Two versions of such a Langmuir probe were used, both of which have observed electron holes. The first version (the "60 μm probe") [6], was constructed from micro-coax with short (~ 0.5 cm) lengths of 60 μm Cu wire (2.5 mil), soldered directly to the center conductor of micro-coax. The Cu wire was covered in a thin ceramic tube, leaving the last 1 mm of the tip exposed to plasma. Four such probe tips were epoxied at fixed separations, and could be rotated such that the probe tips were aligned parallel or perpendicular to the magnetic field. In the second version (the "300 μm probe"), the probe tips were simply the center conductors of the same micro-coax. The geometry and spacing of the various tips of the probe could be reconfigured in a vacuum break since the micro-coax is only semi-rigid. Two geometries of probe tips were deployed, first a "fan" configuration with the tips arrayed over a few-cm of area in the poloidal plane to observe the overall spatial characteristics of the plasma turbulence; and second a "correlation" config-

uration with multiple probes aligned along the field at separations of 4 mm to 1.3 cm.

In all designs the coax lines were shielded from plasma using ceramic tubes and teflon sleeves. The lines were brought out the vacuum chamber through vacuum-compatible SMA feedthroughs. The total length of coax from probe tip to digitizer was about 2 m, and care was taken to make sure that the lengths of all lines were well matched.

The probes were typically used with a load circuit consisting a 4 nF RF blocking capacitor in series with the digitizer 50 Ω load. In this configuration, the probe self-biases to the floating potential over time scales of order $R_p C_b$, where R_p is the "plasma resistance" of the Langmuir probe, approximately the inverse of the slope of the I-V curve at the bias point, and C_b the blocking capacitor. Since R_p will typically be larger than the 50 Ω load, the probe primarily measures changes in probe current on short timescales, converted to a voltage at the scope by 50 Ω, and it is therefore a "floating-current" probe. The design achieves high-bandwidth through its simplicity, but a drawback is the lack of absolute calibration of the measured signals, because the R_p is always imprecisely known.

Two high-bandwidth, digitizing oscilloscopes were used over the course of the experiments, Tektronix model 7254 (5 GS/s sampling, 2.5 GHz analog bandwidth), and Tektronix model 72004 (up to 50 GS/s sampling, 16 GHz analog bandwidth). Both models observed electron hole structures, at greater fidelity by the faster oscilloscope. While Langmuir turbulence has been studied for decades, digital oscilloscopes with high bandwidth and digitization rates (> 1 GHz) and long record lengths (~ 1 MSample) have only recently become available. This allows direct, time-domain study of fast plasma turbulence over the long timescales characteristic of macroscopic plasma phenomena such as the the reconnection events. This proved essential for the identification of the electron holes reported here.

III. OBSERVATION OF ELECTRON HOLES

Figure 2 shows a typical set of observations from a discharge where holes where observed in concert with a reconnection event. Arrays of magnetic flux loops measure the dynamics of the magnetic field at ~ 3 cm resolution over the poloidal cross section, and at temporal resolution of order 1 μs, over the course of a discharge which lasts ~ 2 ms. The fast Langmuir probes study fluctuations over much smaller spatial scales (1 mm) and at fast time scales (500 ps) characteristic of the electron holes.

Figure 2(a) shows the device cross section, with curves showing the magnetic flux surfaces Ψ, and color indicating $d\Psi/dt$; (b) shows the plasma current density evaluated at the x-line; and (c) shows the inductive component of the toroidal electric field. The electric field is observed to peak near the x-point during the reconnection event

(which in this discharge peaked at $t = 1355$ μs), while the plasma current density at the x-point drops by about 40%. Figure 2(d) shows the current density measured by a gridded energy analyzer probe which corresponds to the tail of the electron population at a number of voltage biases. The current of electrons in the tail is observed to increase during the reconnection event.

Simultaneously, fluctuations were observed using the 300-μm probe and Tektronix 72004 oscilloscope. The probe tip locations are indicated in the profiles of Fig. 2(a) by the crossed circles. Three of the probes were collinear in the toroidal direction thus are atop one another in the poloidal projection shown. Fig. 2(e) shows the fluctuation spectrum power (summed over the wide frequency band f_{LH} to f_{ce}), which is observed to strongly increase during the reconnection event. Figure 2 (f) shows the raw fluctuation traces of the fast Langmuir probes for $t = 1350$ to 1370 μs, near the reconnection event. Even at this level of zoom, positively skewed spikes are apparent in the fluctuation trace. Figure 2 (g) zooms further in on the fast Langmuir signals for $t = 1360$ to 1360.5 μs, showing individual spikes.

Figure 3 shows statistics of the fast Langmuir probe signals over the time window 1355 to 1363 μs, using a histogram (a) and power spectrum (b). The power spectrum (b) shows a wide-band character which begins to roll off at ~ 800 MHz, which is approximately the inverse time-width of the spikes. The noise floor is reached near 3 GHz, which is very close to the electron cyclotron frequency of 2 GHz. The histogram (a) shows a skewed distribution of fluctuation voltages with a positive tail of outliers. The outliers are the holes. The skewness of the distribution is a measure of the strong deviation of the fluctuations from the quasi-linear "random phase" state. Were this the case, and if the turbulence were simply a broadband collection of uncorrelated waves, then the distribution of voltage measurements would be gaussian. The presence of skewed fluctuation distributions reflects the correlation between the the frequency components of the signal across the frequency spectrum; the relative phases must be correlated so that (when taking the inverse Fourier transform) they can sum coherently to form a sequence of positive, delta-function-like spikes.

One final observation, typical of observations over many discharges, is apparent in the figure: the regions of plasma with holes vs. without holes have a very narrow spatial structure. In these observations, two probes (yellow and blue in Fig. 2) were only separated by about 2 cm in the poloidal plane, yet the blue probe observed an order of magnitude larger fluctuation power (e) and substantially more holes in the time-domain trace (f). By way of comparison to other plasma scales in VTF: this is of order the ion-sound gyro radius $\rho_s \sim 4$ cm, itself comparable to the width of the current sheet [7]. Finally, it is also comparable to gradient scale lengths observed in the fast electron population, measured with a multi-channel energy-analyzing probe [23].
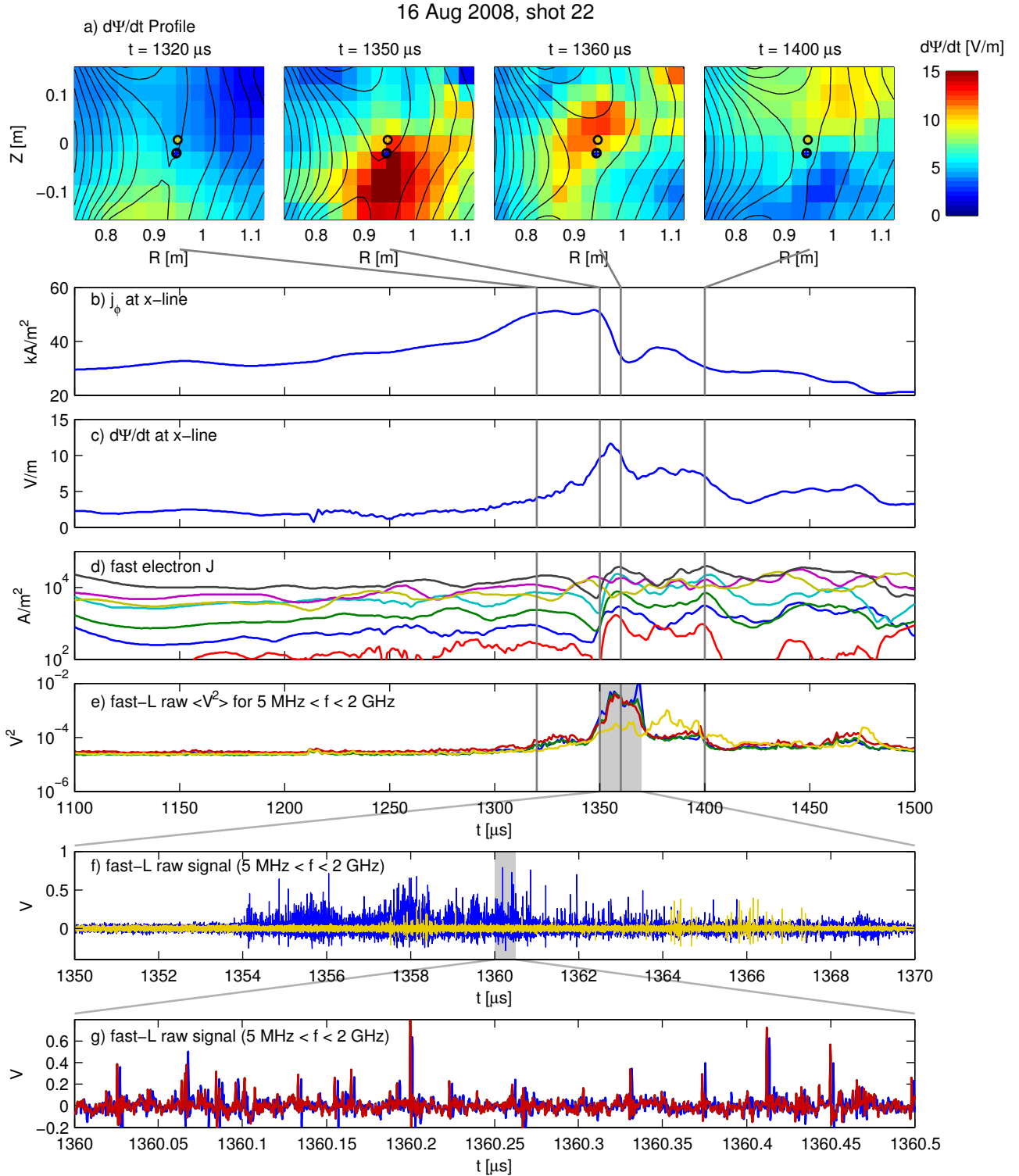
A sequence of experiments was performed, scanning

FIG. 2: (Color online) Observations of electron holes during reconnection events. (a) 2-d contours of flux surfaces Ψ with color indicating $d\Psi/dt$. b) Plasma current density evaluated at the x-line (c) Associated inductive, toroidal electric field $\partial\Psi/\partial t$, evaluated from the flux probe measurements. (d) current density measured by fast electron probe, for biases -140 to -40 V with respect to ground. (e) Fluctuation power measured by fast Langmuir probes. Red, green, and blue traces are from probes collinear in the toroidal direction, whereas the yellow probe is alone. The location of the probes in the poloidal plane is marked in (a). (f) Zooms in on fast Langmuir signal for $t = 1350$ to 1370 μs, near the reconnection event. (g) Further zooms in on fast Langmuir signal for $t = 1360$ to 1360.5 μs, showing individual spikes.
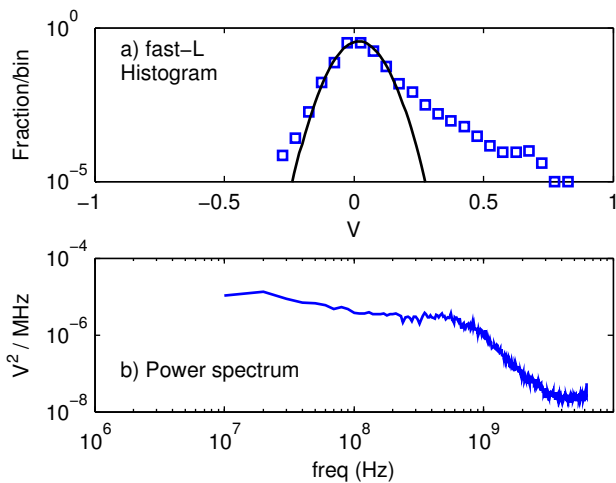
FIG. 3: Statistics of raw fast Langmuir signals over the window $t = 1355$ to 1363 μs. (a) Histogram of measured voltage. showing clear non-Gaussian tale of positive fluctuation events. (b) FFT Power spectrum over the same time window, showing wide-band character out to $\sim$800 MHz.

the position of the fast Langmuir probe to look for correlation of hole observations with landmarks such as the current sheet, the reconnection separatrices, or regions of toroidal strong electric field. However, no strong and repeatable pattern was discovered. Subsequent experiments [21, 22] have shown additional strong toroidal localization of the reconnection events in VTF. A varying toroidal phase of reconnection onset, combined with the observed narrow scale widths of regions with and without holes, suggest (in retrospect) why it might be so difficult to find a pattern from these scans.

IV. DETAILED ELECTRON HOLE MEASUREMENTS

In this section, individual spikes are studied. By observing the spikes on multiple probes arrayed along and across the magnetic field, properties of the holes such as the size parallel and perpendicular to the magnetic field, and their speed (predominantly along the magnetic field) are measured.

Holes have been observed with both 60-μm and 300-μm probes. The original measurements of the key properties of the spikes was accomplished with the 60-μm probe array and Tektronix 7254 oscilloscope [6]. This section will we also include measurements made using the flexible 300-μm probe array and Tektronix 72004 oscilloscope.

Figure 4(a) shows a short, 10 ns time window of fluctuation measurements during a period of spiky turbulence. The window shown contains two spikes; the blue and green traces are on two separate probes, separated by 4.6 mm in the toroidal direction. The data points, sampled at 5 GS/s, appear as open symbols. Notably, the
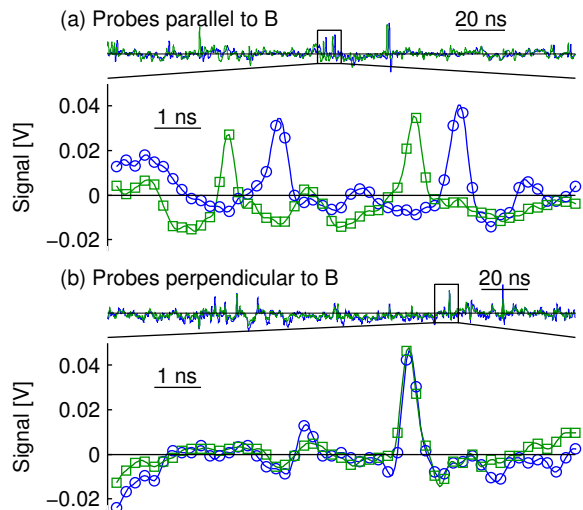

FIG. 4: (Color online) Time traces of spikes moving past a pair of fast Langmuir probes, over 100 ns and then zoomed-in on a 10 ns interval. In (a), the probes are separated by 4.6 mm parallel to the magnetic field. In (b), the probes are separated by 0.8 mm perpendicular to the field.
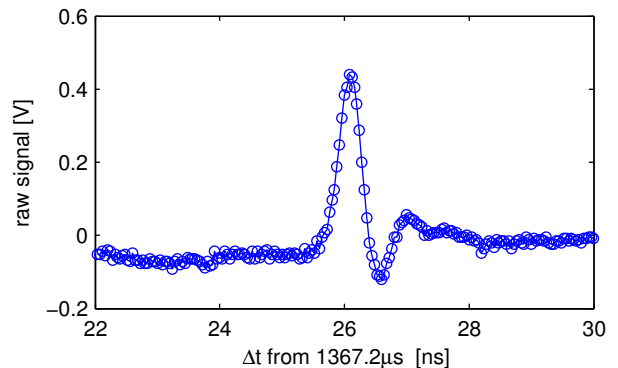

FIG. 5: Time trace of a single spike, digitized at 25 GS/s with the 72004 oscilloscope and the 300 μm probe.

spikes are well-correlated between the two probe tips, but with a time delay (here about 1.2 ns). Other tests with the probes separated perpendicular to the magnetic field, shown in Fig. 4(b), show zero time delay. Therefore, the spikes appear to travel *along* the magnetic field. Furthermore, in Fig 4(a), the green trace (square symbols) is from the "upstream" probe—upstream in terms of the electron flow inferred from the total plasma current—indicating that the spikes travel along the magnetic field *with* the electron flow.

Figure 5 shows additionally an example of a single spike digitized with the 72004 oscilloscope at 25 GS/s. The individual samples are represented by the open circles, separated in time by 40 ps. A negative "tail" can be seen on the spike trace; these are seen on many of the
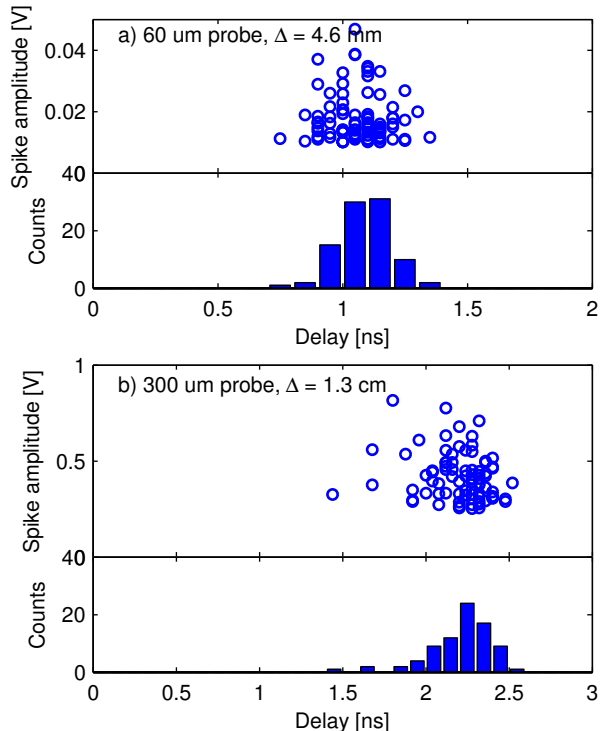
FIG. 6: Probe-probe delays determine the parallel propagation speed of the spikes. (a) Measurements with the Tektronix 7254 scope and 60-μm probes, with probe separation of 4.6 mm. Inferred speed = 4.6 mm/1.1 ns = 4×10^6 m/s. (b) Measurements with the Tektronix 72004 scope and 300-μm probes, with probe separation of 1.3 cm. The range of inferred speed, including uncertainty in the probe separation is $6 \pm 1 \times 10^6$ m/s.

FIG. 7: Measurement of the spike parallel size from time width (fwhm) of spike traces.

spike traces, and it is likely due to a capacitive component of the plasma-probe coupling. No high-frequency oscillations within the spike are observed.

A. Velocity

The propagation speed of the spikes is measured from time delays between spikes events on two probe tips. The histogram in Fig. 6(a) shows the distribution of measured delays for all spikes observed during this discharge; the typical delay between the two probes is about 1.1 ns. Based on the 4.6 mm probe separation, we find that the spikes travel approximately 4×10^6 m/s. In plasma units this is approximately 1.5–2 v_{te}, where $v_{te} = \sqrt{2kT_e/m_e}$ has been evaluated using the typical temperature of 15 eV. Similar measurements have been repeated with the Tektronix 72004 oscilloscope. An example is shown in Fig. 6(b), where we find a similar, superthermal speed of 5.5×10^6 m/s.

Finally, the excellent correlation of the spikes between probe tips at 1.3 cm separation indicates that any per-
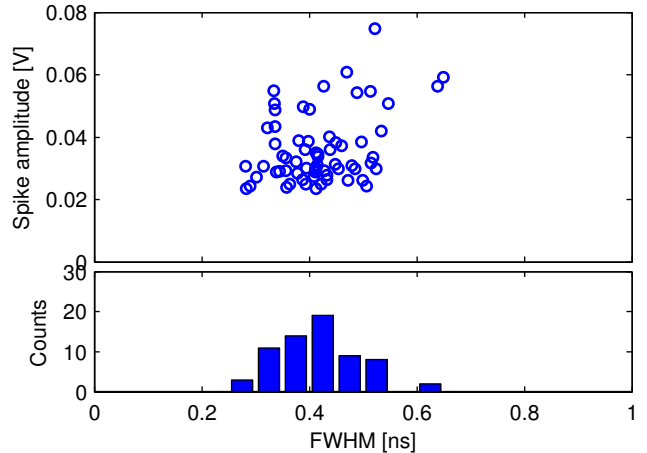
pendicular speed to the hole structures is small, at least less than ~1/6 of the parallel speed (using a typical perpendicular size of 2 mm, found below), and likely much lower. The time delay between observation on separated probes also indicates that these holes persist for at least 2 ns, which is ~25 ω_{ce}^{-1} or 125 ω_{pe}^{-1}; likely this is a relatively weak lower bound and they persist much longer.

B. Parallel size

The parallel size of the spikes (parallel to **B**) is estimated based on the inferred speed and the temporal width of the trace. The spikes from Fig. 4 have full-width-half-maximum (fwhm) temporal widths of about 500 ps. Figure 7 shows the statistics of the parallel widths measured for all spikes found during this discharge; the typical temporal width is about 400 ps. Combining this typical width and the spike velocity, we infer a typical parallel diameter of 1.5 mm. In plasma units, this is ~12 electron gyroradii ($\rho_e = \sqrt{m_e kT_e/e^2B^2} \approx 130$ μm). Alternatively, this is about 60 Debye lengths ($\lambda_D = \sqrt{\epsilon_0 kT_e/ne^2} \approx 25$ μm).

These measurements are repeated with the 300 μm probe and Tektronix 72004 oscilloscope and . Figure 8 shows an example color histogram of electron hole traces stacked atop one another. The color indicates the fraction of traces which crossed a given bin in Δt-ΔV. Holes were selected based on having a peak voltage amplitude between 0.4 and 0.6 V, and the time traces were aligned to have the voltage maximum at $t = 0$. Further cuts were performed to find only isolated spikes, and a linear voltage background was subtracted off based on the levels far from the spike. One observes that the holes here have a typical FWHM of about 0.35 ns, and with this FWHM maximum measurement, combined with the velocity measurements, one infers again a typical parallel
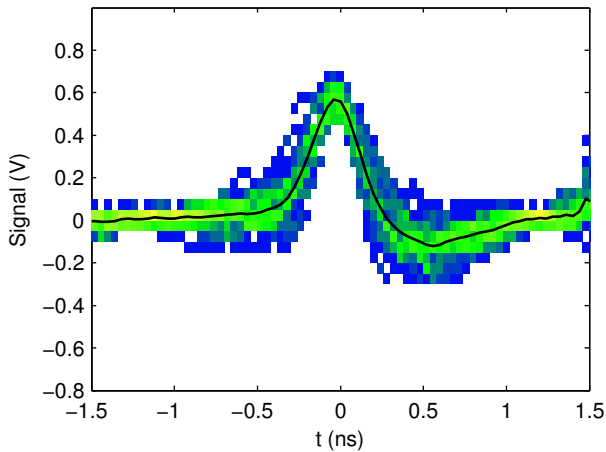
FIG. 8: (Color online) Color histogram of average spike shapes during a discharge, normalized to the same peak voltage. The color indicates the fraction of traces which crossed a particular Δt-ΔV bin. The traces were measured with the Tek 72004 scope, and the impulse response of the coax lines has been deconvolved from the signals.
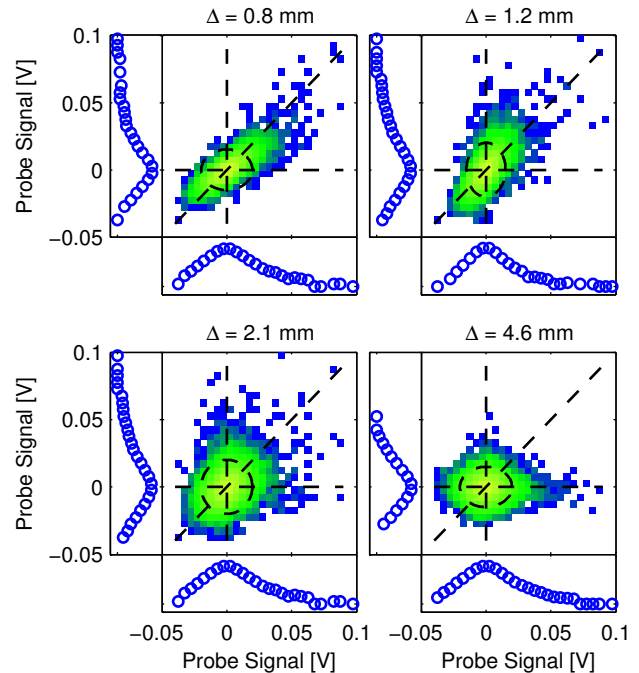

FIG. 9: (Color online) Spike perpendicular size inferred from perpendicular correlation. Probe-probe correlation histograms, and corresponding single-probe log-histograms, at zero time delay. The probe separations range from 0.8 mm to 4.6 mm perpendicular to the magnetic field. Excellent correlation is seen at 0.8 mm separation, and none at 5 mm, bracketing the perpendicular size at about 2 mm.

hole diameter of about 2 mm. Note that this is substantially larger than the probe diameter (300 μm), so finite-probe size effects are minor, potentially affecting this result only at the 10% level. Furthermore, the time-width of the hole trace is substantially longer than the rise time of the 72004 oscilloscope, so the holes are very well resolved by this instrument. Some further tests and analysis was conducted on the finite rise-time effect of the coax line; this is found to have only a very minor quantitative effect on the spike shapes.

C. Perpendicular size

The perpendicular size of the spikes is measured in experiments with the probe tips separated perpendicular to the magnetic field. Figure 9 shows histograms comparing signals observed by pairs of probes at zero time delay. Integrating in the vertical or horizontal directions on any plot gives the single-probe histograms, which are shown in log scale exactly as in Fig. 3(a). As noted before, the tail of outliers on the scatter plots and log-histograms (where the log-histograms deviate from being parabolic) are the holes. As is readily visible from the plots, the holes at $\Delta = 0.8$ mm (top-left) are highly correlated, implying the spikes must be typically larger than 0.8 mm. The same exercise can be repeated for increasing probe separations. Of note, at $\Delta = 4.6$ mm (bottom-right), there is essentially no correlation between the outliers, so the holes are clearly smaller than this. These measurements thus bracket the typical perpendicular diameter of the spikes, which we take as 2 mm. As this is similar to the parallel size, the spikes are approximately spherical.

D. Peak electron hole potentials

We seek to make an estimate of the peak electric potential associated with the hole structures. To do so requires a model to connect the measured signal δV_s to fluctuations in the plasma.

The fast Langmuir probe results presented use a "floating-current" topology, with a load circuit consisting of an RF blocking capacitor in series with the digitizer 50 Ω matched load. On the fast time scales of the electron hole waveforms, only the latter is relevant, and thus the oscilloscope measures $\delta V_s = 50\Omega \times \delta I$, where δI is the fluctuating current into the probe. Furthermore, 50 Ω is a small resistance, so that $50\,\Omega \times \delta I$ does not substantially alter the probe bias (i.e. $V_s \ll T_e$), so that on these fast time scales the plasma sees the probe as a current sink at fixed bias. This model can be immediately observed to have the correct trend with respect to the two probe designs: the typical hole waveforms observed with the 300 μm probe are about a factor of 10–20 larger than those observed with the 60 μm probe (see Fig 6), reflecting the larger collecting area (both diameter and length).

How does a transiting electron hole cause a fluctuation in probe current? The simplest estimate is to consider

the changing plasma potential $\delta\phi$, which shifts the probe I-V curve back and forth, changing the current into the probe. For sufficiently small fluctuations, one linearizes around the bias point; this gives an effective "plasma resistance" R_p coupling from probe to plasma (such that $\delta I = \delta\phi/R_p$); in this case the voltage measured at the scope will be fluctuating plasma potential divided by the ratio $50\Omega/R_p$. With the probe biased to near the floating potential, R_p has magnitude kT_e/eI_{si}, the plasma temperature measured in eV divided by the probe ion saturation current. A typical estimate for the 300 μm probes was a ratio of about 40, leading to a estimated voltage fluctuations of order 10-40 V for the range of spike sizes observed. Therefore we estimate that the holes have amplitude $e\phi$ of order kT_e.

Note there are substantial uncertainties associated with this estimate. First, the plasma-probe coupling resistance R_p is a function of the plasma parameters, and therefore changes throughout the discharge. The temperature in particular is observed to increase substantially (by a factor of 2) during the reconnection events. Second, R_p also depends on the bias voltage of the probe relative to the plasma potential, and for example if the probe deviates by one T_e, then R_p will change by a factor of 3. The floating and plasma potential is observed to change dramatically during the reconnection events [22], and the probe bias will not follow these instantaneously due to the finite time to charge the blocking capacitor and coax line. Finally, for hole potentials beyond kT_e, the linearized probe response itself breaks down (leading in fact to an underestimation of the hole potential).

E.   Observation summary

In summary, we have measured spiky, positively skewed turbulence driven near the current sheet during the reconnection events. The present study of individual spikes finds that they travel along the magnetic field at superthermal speeds, roughly twice the electron thermal speed. The spikes correspond to positive-potentials. They are a few electron gyroradii in diamter, or, equivalently, $\sim$60 Debye lengths. Their aspect ratio (ratio of diameter parallel vs. perpendicular to the magnetic field) is approximately one. The amplitude of the spikes appears to be large and of order kT_e, but this last estimate is highly uncertain owing to limitations inherent in the probe design. Based on their positive potential, which is of large enough amplitude to trap a large fraction of electrons, these structures are identified as electron phase space holes.

V.   DISCUSSION

A.   Comparison with other observations and electron hole theories

The spikes measured in VTF fit well into the framework of electron hole theories. First, we observe positive-potential structures, which is consistent with holes, as positive ϕ is required to trap electrons. Further, electron holes have been documented in many simulations to be the preferred nonlinear structure that grows in the plasma as a result of a strong instability. The observations also are inconsistent with other nonlinear plasma structures (such as solitons) as is discussed in greater detail below. Some aspects of the spikes agree well with the available theory for 3-D electron holes, for instance, such as the typical width of a few gyroradii. On the other hand, their parallel size is large, and they travel quickly compared to available theories, points which are addressed below.

First, the typical perpendicular size of the observed electron holes (a few ρ_e) is in agreement with available space observations and simple theoretical considerations. Franz _et al._ [24] have presented a statistical study of the inferred parallel and perpendicular sizes of electron holes measured by the POLAR spacecraft. The critical parameter here is ω_{pe}/ω_{ce}, or equivalently, ρ_e/λ_D. They found that the perpendicular size changed from being a few λ_D when $\omega_{pe}/\omega_{ce} \leq 1$ to being a few ρ_e when $\omega_{pe}/\omega_{ce} \geq 1$. This concurs with our measurements of ρ_e-scale holes, as VTF is in the latter regime, $\omega_{pe}/\omega_{ce} \sim 5$.

Theory also predicts that the ρ_e scale sets a minimum perpendicular size: holes depend on a positive potential causing depletion of electrons, which results only when the electrons obey a magnetized, 1-D response along the field lines. This issue has been discussed by a few authors, for example Ng and Bhattacharjee [25], who provide essentially a proof that 3-D holes with unmagnetized electrons do not exist. To keep the electrons magnetized, the hole's perpendicular size must be at least a few gyroradii. Other work [26] has also studied the _stability_ of holes in weak magnetic fields, finding that holes must be multiple gyroradii in diameter for stability, in addition to equilibrium.

While the perpendicular size seems to be in agreement, the parallel size is larger than most space observations. The typical _parallel_ size of holes observed by spacecraft [13, 14, 24] is nearly always a few Debye lengths. This is much narrower than the holes we have observed, which are roughly 60 λ_D wide (FWHM) However, holes this wide are not theoretically forbidden: in fact, calculations show that holes become wide ($\gg \lambda_D$) when they move at high speeds ($v_{hole} \approx v_{te}$) [27]. This is qualitatively consistent with the measurements here in that we observe holes that are both wide and fast. Recent electron hole observations on the LAPD device have measured holes with half-widths clustered around 10 λ_D (yielding full-widths of 20 λ_D). These holes were observed in the

complementary plasma regime $\omega_{pe} < \omega_{ce}$, with speeds of 0.9 to 1.6 (recalculated in terms of the thermal speed definition $(2kT/m_e)^{1/2}$) [12].

Interestingly, based on available theories, the holes appear to move *too* fast. Schamel's limit [2] (also found by Goldman [27]) for instance is that the speeds should be less than $0.9 \times v_{te}$, whereas we observe closer to $2 \times v_{te}$. Of course, this is evaluated with the typical electron temperature of 15 eV. Electron heating, including tail energization has been observed during the reconnection events to temperatures near 30 eV, but this still leave the holes superthermal. It is important to note, however, that the hole structures are quite localized, whereas the temperature measurements are always over larger spatial regions and at slower time scales, so it cannot be excluded that there are local regions of even higher temperatures. Furthermore, the holes themselves will strongly churn the particle distributions especially if the amplitudes are as large as estimated, so it may well be that locally the above conditions are satisfied.

Finally, recent THEMIS observations [18] show holes with remarkable similarity to those observed here. These observations found holes that moved at roughly $2v_{te}$, were wide in the parallel direction (many 10's of λ_D), and possessed peak potentials of order kT_e. These holes were also elongated, with $L_{||} > L_\perp$, whereas the VTF holes appear to be more spherical. However, the two systems are not in identical regimes, with $\omega_{pe}/\omega_{ce} \sim 5$ for VTF vs. ~ 1.5 for the THEMIS observations. Thus the gyroradius is relatively larger in VTF, and so if a few gyroradii still sets the minimum hole width, then the VTF holes would be wider and therefore more spherical.

One important consequence of the fast velocity of these plasma structures is that they likely do not evolve out of Buneman instability, as did the electron holes observed in recent reconnection particle simulations [19]. The Buneman instability is a slow mode, with phase velocities of order a few times the ion sound speed, whereas the superthermal hole speeds observed are much faster than this. Buneman instability also requires a large electron drift speed, $v_{de} > v_{te}$ for linear instability. It is difficult to imagine this situation prevailing in these experiments, as the typical electron-ion drift speeds are only 10-20% of the electron thermal speed. These drifts are inferred from plasma current measurements, over scales of about 3 cm resolution, and therefore do not constrain substantially narrower filaments where such drifts could arise.

The holes instead seem much more likely to be driven by *electron-electron* instabilities, i.e. bump- or beam-on-tail. In fact, recent 3-D reconnection simulations from Che *et al* [20], have found both slow holes from Buneman instability at early times, and the additional formation of superthermal holes from electron-electron instabilities at later times.

However, it is important to point out that both of these simulation studies were in a regime $\omega_{pe} < \omega_{ce}$, which is the opposite ordering of VTF. This low density in the computational studies is consistent with a relatively large electron drift velocity, large enough to drive the Buneman instability in the initial condition. It would be therefore of great interest to extend these computational studies to the VTF regime, which still has a strong guide field, but is at high density ($\omega_{pe} \gg \omega_{ce}$) and at low average electron drift speed ($v_{de}/v_{te} \sim 0.1$)

B. Comparison with other theories for nonlinear plasma structures

We have found good agreement with the electron-hole based theories. In this section, we compare with other known types of nonlinear plasma structure. Besides hole structures, which rely on the nonlinear effect of particles trapped in the wave, other nonlinear theories involve either high-frequency pump waves (e.g. "envelope solitons") or other nonlinearities in the fluid equations (e.g. standard KdV solitons)

Envelope solitons are formed through the nonlinear interaction of a high frequency "pump wave" and a low frequency envelope [28]. If the pump-wave attains large amplitude, it can expel plasma through the pondermotive force. If sufficient plasma density is repelled, the local dielectric properties of the plasma are changed, trapping the high frequency wave and creating small regions ("envelopes") of intense, strong waves. If this is the source for the structures observed in VTF, the spikes would ostensibly be the envelopes, with a high-frequency wave inside the envelope as the pump (in the magnetized context they are upper-hybrid waves). Previous theories [29] have focused on coupling upper-hybrid waves to very low-frequency envelopes such as a Alfvén waves; this would need to be revisited to determine if a theory can be constructed that couples to *electron*-scale envelopes.

However, we also have not observed any such high frequency components inside the spikes (by a ratio of at least 50: $V_{rms} \simeq 0.008$ V for $f > 2$ GHz, vs. 0.4 peak V for the spikes, see Fig. 5). This despite nominal pump wave amplitudes which should be of order or larger than than the envelope. While certainly the probe system will be less sensitive to these high-frequencies (f_{uh} is estimated to be $\sim$10 GHz), we cannot find reason for a factor of 50 attenuation beyond the response at the spike frequencies.

A second class of nonlinear plasma structures do not involve high-frequency pump waves, but instead other nonlinearities in the fluid equations. These are mathematically akin to the classical Korteweg-de-Vries solitons. In these structures, a wave-steepening effect associated with the nonlinearity balances with wave dispersion to yield a coherently propagating structure. In plasma, these include ion acoustic solitons, *electron* acoustic solitons, Alfvén solitons, and drift wave solitons (for a review, see [30].) Most are not relevant to the present measurements and can be immediately discounted based on characteristic speed and wavelength.

One which comes closest to matching our observa-

tions are Trivelpiece-Gould solitons, first observed and described theoretically by Ikezi and collaborators [31]. Such structures were first found in discharge tube experiments, in fact in the same laboratory experiments which first studied electron holes. The holes and solitons could could be distinguished in the experiments by the sign of ϕ; the holes had $\phi > 0$ consistent with particle trapping, and the solitons $\phi < 0$. The sign of ϕ for the TG soliton follows because they depend on electron compression (in the nonlinear continuity equation) for the nonlinearity.

Another potential candidate, electron acoustic solitons [32], requires the separation of electrons into separate "hot" and "cold" electron populations, (satisfying $T_c \ll T_h$, and $n_c \lesssim n_h$), and allows solitary structures with speeds above the electron acoustic speed $v_{ea} = (n_c/n_h)^{1/2}v_{th}$. Classical EA solitons are also compressive and have $\phi < 0$. However, some recent work has constructed EA soliton structures by incorporating a third electron "beam" component, and which can now have positive or negative potentials depending on parameters [33]. The principle difficulty with the EA soliton hypothesis for the VTF observations, however, is again that exclusively positive potentials are observed, and that a cold electron population has not been observed and would be thermalized in about one electron collision time, which is of order microseconds.

One other difference between classical solitons and electron holes is the existence of one-to-one relations between amplitude, velocity, and width in the former but not the latter. This results from the substantially larger parameter space for electron holes, owing to freedom in the number of trapped electrons. (The beam-driven EA solitons also have more freedom, due to extra freedom due to the beam [33].) Of note here, our measurements (see Figs. 6 and 7) also do not show any discernible amplitude-velocity or amplitude-width relationship. Of course, it is also very difficult to exclude such a relationship, since the probes are smaller than the holes and therefore can potentially miss the peak potential on the axis of the hole.

C. Electrostatic vs. electromagnetic response

This section considers the dominant electric field physics for the observed holes, namely whether they are predominantly electrostatic or electromagnetic phenomena. Interestingly, recent magnetospheric observations from the THEMIS spacecraft have found magnetic perturbations inside large-diameter, superthermal holes [18]. As these observations otherwise appear to be very similar to the VTF holes, it is of interest to estimate what these electromagnetic effects could be in VTF. Note that directly observing magnetic fluctuations inside holes in VTF (using magnetic pickup coils) would be extremely difficult based on the required small size (1 mm) and fast time response (∼GHz).

Electrostatic and electromagnetic wave phenomena in plasmas are distinguished by the dominant physics for generating the electric fields associated with the wave. For electrostatic waves, the dominant plasma response is to be bunched by the electric field, and to therefore create electric fields via a small amount of charge separation. In contrast, for electromagnetic waves, the dominant plasma response is electric current, which then accounts for the wave electric field by induction.

Here we show from the measurements plus scaling estimates that that the VTF holes observed are predominantly electrostatic. This does not rule out small magnetic fields generated by the currents associated with electron motion in the hole, it merely argues that any such magnetic fields are not a dominant physics effect determining the electric field structure of the hole.

Following standard procedure, combining Ampere's and Faraday's laws, the electric field associated with a wave will satisfy

$$\nabla \times \nabla \times \mathbf{E} = -\mu_0 \frac{\partial \mathbf{j}}{\partial t} + \frac{1}{c^2} \frac{\partial^2 \mathbf{E}}{\partial t^2}. \tag{1}$$

The electrostatic limit of this equation is well-known, but subtle [34]. Electrostatic phenomena satisfy $\mathbf{E} = -\nabla \phi$, leaving the LHS identically zero. However, the LHS itself is composed of multiple terms which, in the electrostatic limit, are the largest terms and are canceling one another. For this cancellation to dominate, the RHS must be small compared to individual terms of the LHS, so that

$$|k^2||E| \gg \left|\frac{\omega^2}{c^2}\right||E|, |\mu_0 \omega j|, \tag{2}$$

where ω and k are the frequency and wave numbers associated with the phenomena. The second condition is more restrictive for our regime, and the physical content is that the currents associated with an electrostatic disturbance are not sufficient to account for the electric fields by induction.

To complete this analysis, we estimate what currents arise in the plasma due to a transiting electron hole structure in the VTF parameter range and verify that the above conditions are satisfied. We replace k with $1/L$, where L is the characteristic radius of the hole, found to be about 1 mm, or about 5 ρ_e. Similarly, we replace ω with $1/\tau$, where τ is the time for the spike to go past a volume element of plasma. L and τ re related by the hole speed $V = L/\tau$. The analysis is further simplified since we observe that these spikes have roughly unity aspect ratio, so there is only one length scale in the problem.

First, the Maxwell displacement current term can be seen to be small if $L^2/\tau^2 = V^2 \ll c^2$. This is well satisfied, since the observed holes move well below the speed of light, $V/c \sim 1/50$.

Next, we estimate sizes of various currents j on the right hand side. One of the most important of these is the $E \times B$ motion of the electrons in the positive potential of the spike; this carries electrons azimuthally around the spike. (Notably, the magnetic perturbation associated with the THEMIS measurements was attributed to

this current [18].) This effect gives a current neE/B, which is small if $\mu_0 L^2 ne/\tau B \ll 1$. This simplifies to the condition $VL/v_{Ae}d_e \ll 1$, where v_{Ae} is the so-called *electron* Alfvén speed $v_{Ae}^2 = B^2/\mu_0 nm_e$, and d_e is the electron skin depth, $d_e = c/\omega_{pe}$. Current also arises from the electron polarization drift, but this is smaller than the $E \times B$ current, so will also be negligible under the same circumstances.

Finally, we estimate the parallel (to B) currents that arise from kicks to the electrons from the hole electric fields. From the electron parallel momentum equation, this is estimated to be $\Delta v \simeq eE\tau/m_e$, giving a current $ne^2\tau E/m_e$. This will be negligible if $L^2/d_e^2 \ll 1$.

In summary, we are left with two requirements for holes to be electrostatic: $(L/d_e)(V/v_{Ae}) \ll 1$, and $L^2/d_e^2 \ll 1$. The condition (V/v_{Ae}) is well-satisfied in VTF because of the large guide field and small plasma β, since we have shown $V \simeq 2v_{te}$, but $v_{te}^2/v_{Ae}^2 = \beta \sim 10^{-3}$. Finally, $L^2/d_e^2 \ll 1$ follows because $d_e \simeq 5$ mm at $n \simeq 10^{18}$ m^{-3}, so $L^2/d_e^2 \simeq 0.1$.

The condition $L^2/d_e^2 \ll 1$ is analogous to the electrostatic condition $k^2 d_e^2 \gg 1$, which separates the high-frequency electrostatic Trivelpiece-Gould waves, also called electrostatic whistler waves, $(\omega = \omega_{ce}\cos\theta)$ from the standard electromagnetic whistlers $(\omega = \omega_{ce}k^2 d_e^2\cos\theta$, where $\cos\theta = k_{||}/k)$ in the cold plasma dispersion relation [34]. (Both these expressions are in the limit $\omega_{pe} \gg \omega_{ce}$ relevant to these experiments.) This therefore suggests that these electron holes share the dominant linear physics with the TG / ES whistler waves, with the important addition of the non-linear electron trapping physics. In this connection, recent experimental observations of electron holes on the LAPD experiment [12], also concluded that the holes were part of a spectrum of such waves.

Holes and ES whistler waves are also found in close association in many space physics and autoral contexts (e.g. [35, 36]), and ES whistler waves have been shown to be responsible for decay of electron holes formed in simulations of beam-plasma systems [37, 38]. In VTF it was found that during reconnection events where holes were *not* observed, there was nonetheless still substantial electrostatic turbulence in this same frequency range $f_{LH} < f < f_{ce}$ [23], termed "lower-hybrid" modes since the frequency spectrum peaked at a few times f_{LH}. These waves were shown to also be electrostatic, and had similar parallel phase speeds to the hole velocities.

D. Direct electron-ion momentum coupling

In this section, we attempt a calculation of how much *direct* momentum is coupled from electrons to ions via the holes. Because the current carried by the electrons is directly proportional to the total electron momentum, a direct anomalous resistivity effect must remove electron momentum, giving it either to waves or ions. This is the simplest estimate one can make of the possible feedback
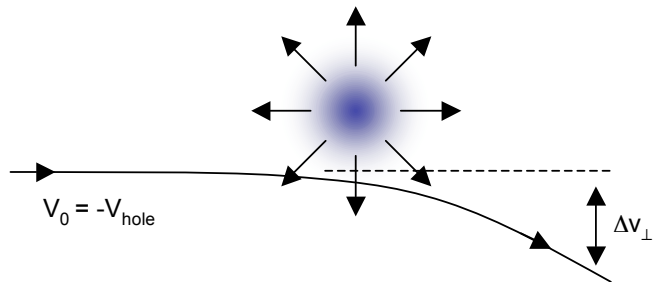

FIG. 10: Hole-ion interaction: ions impinge on the hole at speed $v_0 = -v_{hole}$, where v_{hole} is the speed of the hole in the lab frame. Ions can be taken at rest in the lab frame as the hole velocities are much larger than any ion speed. Through the collision the ions gain a (small) kick $\Delta v_\perp$ and lose a small amount of parallel speed, $\Delta v_{||} \propto \Delta v_\perp^2$.

effect of the holes on reconnection. However, it is but one of many other possible indirect effects, which will be discussed below.

It is found that these holes do not strongly mediate *direct* anomalous resistivity in the plasma. To do so, they will have to effectively kick and transfer momentum to the ions. However, one finds that the ions and holes are weakly coupled due to the fast speed of the holes. This causes the hole-ion interactions to become a weak, diffusive interaction, and the associated momentum transfer is estimated to be weak.

To estimate the rate of momentum transfer to ions from the holes, we estimate the change in ion parallel velocity $\Delta v_{||}$ per hole encounter. This is most easily calculated in the hole reference frame, in which the ion will impinge with a relative velocity $v_0 = -v_{hole}$. A similar technique was used by Ergun *et al* [14] to estimate the coupling of ions to electron holes observed by the FAST satellite in the auroral upward and downward current regions; a schematic of this process is shown in Fig. 10. Conservation of energy through the collision gives $2v_0\Delta v_{||} = -\Delta v_\perp^2$. Assuming weak coupling (verified *a posteriori*), $\Delta v_\perp$ can be estimated based on a straight-line orbit past the hole to be

$$\Delta v_\perp \sim \frac{e}{m_i}\int dt\,\nabla\phi \sim \frac{e}{m_i v_0}\int d\ell\,\nabla\phi \sim \frac{e\phi_0}{m_i v_{hole}},$$

where ϕ_0 is the peak potential associated with the hole. We have also used the fact that the holes have approximately unity aspect ratio in estimating the integral.

Letting the ion strike r holes per second, we find

$$E_{eff} \sim \frac{m_i}{e}r\Delta v_{||},$$

$$\sim r\frac{e\phi_0^2}{m_i v_{hole}^3}.$$

This expression can be seen to be analogous to the momentum coupling from quasi-linear diffusion [39] due to fast-phase-velocity linear modes, with the mode growth

rate γ replaced by the rate of holes r and the wave phase velocity by v_{hole} .

Based on this estimate, the momentum transfer from holes to ions is very small, corresponding to $\ll 0.1$ V/m (versus peak reconnection electric fields of 15 V/m.) This estimate is based on peak hole rates of 20 holes/μs, hole potentials of order 20 V, and hole velocities of order 5×10^6 m/s. Again, the root of the weak coupling is $e\phi/m_i v_{hole}^2 \approx 2 \times 10^{-6} \ll 1$; the ions have a very large amount of energy in the hole frame.

The direct resistivity effect is but one of many effects that the holes can play in the reconnection region. For instance, the holes certainly mediate strong momentum coupling from electrons to electrons (consider electrons trapped inside the hole, whose momentum reverses at each bounce). However, since the total momentum in the electrons will not be changed by electron-electron coupling, neither will the plasma current drasticly change. Note that electron-electron coupling does have the effect of modifying the electron distribution to rein in a run-away tail and thus overall be more collisional. However, to explain reconnection rates in VTF with an anomalous resistivity requires a large gain over the collisional resistivity (of order 10), so such an effect is clearly not sufficient.

Future work should continue to study the cause and effect between holes, fast electrons, and magnetic reconnection. In our simple estimate, the observed holes will not likely contribute to substantial *direct* anomalous resistivity to the plasma, as their high velocity will limit interaction with ions. Instead, since the holes likely evolve from strong electron-electron instabilities they will primarily transfer momentum from fast to slow electrons.

VI. CONCLUSIONS

In this paper we have reported on detailed experimental studies and identification of electron holes created during magnetic reconnection events. The observation of strong, nonlinear turbulence suggests that the reconnection events are creating sharp beam-on-tail velocity space structures, which produce large amplitude turbulence with strong growth rates sufficient to trap resonant electrons within the wave troughs.

Observations were presented which used substantially faster digitizing hardware, and which confirm the previous observations of large parallel diameter and fast, superthermal phase speed. Detailed study of individual holes has found that in the VTF plasmas, characterized by dielectric constant $\omega_{pe}/\omega_{ce} \approx 5$, the typical size of the holes is a few ρ_e, or many 10's of λ_D, with roughly unit aspect ratio parallel and perpendicular to the field. The perpendicular size is in agreement with recent space observations and supports the idea that holes must always be at least a few ρ_e wide in order to retain magnetized electron dynamics. The holes were estimated to have a large potential ($e\phi/kT_e \sim 1$). Based on simple scaling arguments, we found that the observed holes are predominantly electrostatic structures, and share substantial linear physics with electrostatic whistlers (equivalently Trivelpiece-Gould waves, electrostatic magnetized plasma waves occupying the region $\omega_{lh} < \omega < \omega_{ce}$, with dispersion relation $\omega = \omega_{ce}k_{||}/k$, again for the relevant plasma regime $\omega_{pe} \gg \omega_{ce}$). Very similar holes were observed recently by the THEMIS spacecraft [18]; they share many properties with the VTF holes such as superthermal speed and large ($\gg \lambda_D$) parallel size.

The holes are strongly associated with electron energization, suggested both by their thermal or superthermal velocities and their connection to reconnection events and subsequent energetic particle production. However, through an estimate of the momentum coupling of holes to ions, we propose that the observed holes do not contribute to substantial *direct* anomalous resistivity in the plasma. Nonetheless, they certainly strongly modify the electron phase space through trapping effects. Finally, these observations imply that the reconnection events, in addition to the heating and energization that can be concluded from the relatively coarse-grained energy analyzer measurements available, are also driving strong electron beams. These beams must be sufficiently sharp in velocity space so that the associated beam-on-tail instabilities saturate by particle trapping and eventually form electron holes. It would be of great interest to obtain through theory and simulation detailed constraints on the conditions required to produce the observed holes, as this would likely produce very useful information on the plasma state and electromagnetic field structures characteristic of reconnection current sheets.

[1] I. Bernstein, J. Greene, and M. Kruskal, Phys. Rev. **108**, 546 (1957).

[2] H. Schamel, Phys. Rep. **140**, 161 (1986).

[3] D. Biskamp, *Magnetic Reconnection in Plasmas* (Cambridge University Press, Cambridge, 2000).

[4] M. Yamada, R. Kulsrud, and H. Ji, Rev. Mod. Phys. **82**, 603 (2010).

[5] J. Egedal, A. Lê, Y. Zhu, W. Daughton, M. Øieroset,

T. Phan, R. P. Lin, and J. P. Eastwood, Geophys. Res. Lett. **37**, L10102 (2010).

[6] W. Fox, M. Porkolab, J. Egedal, N. Katz, and A. Le, Phys. Rev. Lett. **101**, 255003 (2008).

[7] J. Egedal, W. Fox, N. Katz, M. Porkolab, K. Reim, and E. Zhang, Phys. Rev. Lett. **98**, 015003 (2007).

[8] K. Saeki, P. Michelsen, H. L. Pécseli, and J. J. Rasmussen, Phys. Rev. Lett. **42**, 501 (1979).

[9] J. P. Lynov, P. Michelsen, H. L. Pécseli, J. J. Rasmussen, K. Saeki, and V. A. Turikov, Physica Scripta **20**, 328 (1979).

[10] P. Guio, S. Børve, L. K. S. Daldorff, J. P. Lynov, P. Michelsen, H. L. Pécseli, J. J. Rasmussen, K. Saeki, and J. Trulsen, Nonlin. Processes Geophys. **10**, 75 (2003).

[11] J. D. Moody and C. F. Driscoll, Phys. Plasmas **2**, 4482 (1995).

[12] B. Lefebvre, L. J. Chen, W. Gekelman, P. Kintner, J. Pickett, P. Pribyl, S. Vincena, F. Chiang, and J. Judy, Phys. Rev. Lett. **105**, 115001 (2010).

[13] H. Matsumoto, H. Kojima, T. Miyatake, Y. Omura, M. Okada, I. Nagano, and M. Tsutsui, Geophys. Res. Lett. **21**, 2915 (1994).

[14] R. E. Ergun, C. W. Carlson, J. P. McFadden, F. S. Mozer, L. Muschietti, I. Roth, and R. J. Strangeway, Phys. Rev. Lett. **81**, 826 (1998).

[15] S. D. Bale, P. J. Kellogg, D. E. Larson, R. P. Lin, K. Goetz, and R. P. Lepping, Geophys. Res. Lett. **25**, 2929 (1998).

[16] H. Matsumoto, X. H. Deng, H. Kojima, and R. R. Anderson, Geophys. Res. Lett. **30**, 1326 (2003).

[17] C. Cattell, J. Dombeck, J. Wygant, J. F. Drake, M. Swisdak, M. L. Goldstein, W. Keith, A. Fazakerley, M. Andrè, E. Lucek, et al., J. Geophys. Res. **110**, A01211 (2005).

[18] L. Andersson, R. E. Ergun, J. Tao, A. Roux, O. LeContel, V. Angelopoulos, J. Bonnell, J. P. McFadden, D. E. Larson, S. Eriksson, et al., Phys. Rev. Lett. **102**, 225004 (2009).

[19] J. Drake, M. Swisdak, C. Cattell, M. Shay, B. Rogers, and A. Zeiler, Science **299**, 873 (2003).

[20] H. Che, J. F. Drake, M. Swisdak, and P. H. Yoon, Phys. Rev. Lett. **102**, 145004 (2009).

[21] N. Katz, J. Egedal, W. Fox, A. Le, J. Bonde, and A. Vrublevskis, Phys. Rev. Lett. **104**, 255004 (2010).

[22] N. Katz, J. Egedal, W. Fox, A. Le, A. Vrublevskis, and J. Bonde, Phys. Plasmas **18**, 055707 (2011).

[23] W. Fox, M. Porkolab, J. Egedal, N. Katz, and A. Le, Phys. Plasmas **17**, 072303 (2010).

[24] J. R. Franz, P. M. Kintner, C. E. Seyler, J. S. Pickett, and J. D. Scudder, Geophys. Res. Lett. **27**, 169 (2000).

[25] C. S. Ng, A. Bhattacharjee, and F. Skiff, Phys. Plasmas **13**, 055903 (2006).

[26] L. Muschietti, I. Roth, C. Carlson, and R. Ergun, Phys. Rev. Lett. **85**, 94 (2000).

[27] M. Goldman, D. Newman, and A. Mangeney, Phys. Rev. Lett. **99**, 145002 (2007).

[28] M. V. Goldman, Rev. Mod. Phys. **56**, 709 (1984).

[29] M. Porkolab and M. V. Goldman, Phys. Fluids **19**, 872 (1976).

[30] K. E. Lonngren, Plasma Phys. **25**, 943 (1983).

[31] H. Ikezi, P. J. Barrett, R. B. White, and A. Y. Wong, Phys. Fluids **14**, 1997 (1971).

[32] N. Dubouloz, R. Pottelette, M. Malingre, and R. A. Treumann, Geophys. Res. Lett. **18**, 155 (1991).

[33] M. Berthomier, R. Pottelette, M. Malingre, and Y. Khotyaintsev, Phys. Plasmas **7**, 2987 (2000).

[34] T. H. Stix, *Waves in Plasmas* (Springer-Verlag, New York, 1992).

[35] R. E. Ergun, C. W. Carlson, J. P. McFadden, R. J. Strangeway, M. V. Goldman, and D. L. Newman, Geophys. Res. Lett. **28**, 3805 (2001).

[36] J. S. Pickett, J. R. Franz, J. D. Scudder, J. D. Menietti, D. A. Gurnett, G. B. Hospodarsky, R. M. Braunger, P. M. Kintner, and W. S. Kŭrth, J. Geophys. Res. **106**, 19081 (2001).

[37] M. Goldman, M. Oppenheim, and D. Newman, Geophys. Res. Lett. **26** (1999).

[38] M. Oppenheim, D. Newman, and M. Goldman, Phys. Rev. Lett. **83**, 2344 (1999).

[39] B. B. Kadomtsev, *Plasma Turbulence* (Academic Press, London, 1965).